AIP | Physics of Plasmas

Diocotron modulation in an electron plasma through continuous radio-frequency excitation

B. Paroli, G. Maero, R. Pozzoli, and M. Romé

Citation: Physics of Plasmas (1994-present) **21**, 122102 (2014); doi: 10.1063/1.4903847
View online: http://dx.doi.org/10.1063/1.4903847
View Table of Contents: http://scitation.aip.org/content/aip/journal/pop/21/12?ver=pdfcov
Published by the AIP Publishing

Diocotron modulation in an electron plasma through continuous radio-frequency excitation

B. Paroli,[a] G. Maero, R. Pozzoli, and M. Romé
Dipartimento di Fisica, Università degli Studi di Milano and I.N.F.N. Sezione di Milano, Via Celoria 16, 20133 Milano, Italy

(Received 18 September 2014; accepted 23 November 2014; published online 10 December 2014)

The application of a radio-frequency (RF) excitation to any electrode of a Penning-Malmberg trap may result in significant electron heating and ionization of the residual gas with the formation of a plasma column when the RF frequency is of the order or larger than the typical axial bounce frequencies of few-eV electrons. The use of a quadrupolar excitation can induce additional phenomena, like formation of dense, narrow-cross section columns which exhibit an $m_\theta = 1$ diocotron mode, i.e., a rotation of their center around the trap axis. A series of experiments is presented and discussed showing that the continuous application of such excitation causes a dramatic perturbation of the plasma equilibrium also involving continuous production and loss of particles in the trapping region. In particular, the growth of the first diocotron mode is suppressed even in the presence of ion resonance and resistive instability and the mode exhibits steady-state or underdamped amplitude and frequency modulations, typically in the Hertz range. © *2014 AIP Publishing LLC*.
[http://dx.doi.org/10.1063/1.4903847]

I. INTRODUCTION

Penning traps[1,2] have been used for some decades up to now to confine and manipulate particle samples with a single sign of charge in a variety of research and industrial environments. Basic physics applications include low-uncertainty mass spectrometry and metrology,[3–6] storage and production of antimatter at low energy,[7–9] fluid dynamics, and turbulence.[10–15] The Penning trap concept also applies to technological applications like chemical analysis (via broad-range mass spectrometry),[16] Penning gauges, and ion pumps.[17] The confinement principle is simple and robust, and relies on the superposition of an electric field provided by suitable voltages on stacked cylindrical electrodes and an axial magnetic field created by solenoid electromagnets or permanent magnets. Together with ultra-high vacuum (UHV), such scheme would yield a virtually indefinite storage, nevertheless confinement of large samples is limited in time by several practical reasons, e.g., collective processes, collisions, and a number of imperfections including misalignments,[18] resistive-wall dissipation,[19,20] and presence of particles with opposite sign of charge.[21,22] These processes lead either to diffusion or to the rise of instabilities and can be counteracted by active manipulation. An example is the well-known "rotating-wall (RW) technique,"[23] where a radio-frequency (RF) electric drive in the form of a rotating dipole is applied to an azimuthally segmented electrode and angular momentum is transferred to the plasma via resonant coupling to Trivelpiece-Gould modes, so that the transverse size of the sample is reduced and a stable confinement is maintained for very long times even at densities beyond the Brillouin limit. Other mechanisms leading to a damping of transverse instabilities have been observed, as for instance, rotational pumping of cyclotron-cooled plasmas,[24,25] local particle trapping and chaotic neoclassical transport due to electric or magnetic perturbations,[26,27] effective-potential effects of non-resonant, high-frequency transverse excitations,[28] particle flux through the critical layer.[29]

Despite the rich literature about the physics of these machines, large room for investigation is still available. We can cite, for instance, traps where particles of different species or even different signs are present, either due to background gas ionization (and hence being unwanted) or because their simultaneous confinement is required. Examples include formation of antimatter, trapping and cooling of multispecies or dust-contaminated particle samples and plasmas,[30,31] ion pumps.[32] Another case is represented by systems where the equilibrium is strongly altered by external perturbations like RF excitations. We have previously discussed an original case where an electron plasma is generated by the application of a RF drive on an axisymmetric or azimuthally segmented trap electrode.[33] Under suitable conditions, heating of the residual background electrons can lead to significant ionization and to the formation of an electron column with density in the 10^6–$10^7\,\mathrm{cm}^{-3}$ range, i.e., comparable with those obtained by means of conventional thermo- or photocathodes. We present here a further investigation of this novel system, where we observe the suppression of the exponential growth of the $m_\theta = 1$ diocotron instability, accompanied by the occurrence of a frequency and amplitude modulation of the $m_\theta = 1$ mode itself at an extremely low frequency, typically in the Hertz range. Here, the equilibrium is significantly more complicated with respect to the typical unperturbed or weakly perturbed plasma dynamics, as both continuous ionization, electron and ion losses, and electric excitation enter the column radial balance. Specifically, the continuous application of the RF excitation accounts both for the ionization and hence the

[a]Bruno.Paroli@unimi.it. URL: http://plasma.fisica.unimi.it

diocotron mode growth and for the transfer of angular momentum to the plasma via wave-particle interaction. The dynamical equilibrium thus obtained, where the column rotates at a stable, but possibly modulated, offset around the trap axis, can last for hours.

The paper is organized as follows. In Sec. II, we describe the set-up and the experimental procedure. In Sec. III, an analysis and characterization of the low-frequency (LF) modulation is presented. Different regimes are discussed, namely, stationary and damped oscillations. Section IV is devoted to the discussion and assessment of the present work, and finally to a conclusion and outline of future investigations.

II. SET-UP AND EXPERIMENTAL PROCEDURE

The experiments are performed in the ELTRAP (ELectron TRAP) Penning-Malmberg device, whose main elements are sketched in Fig. 1. A 1260 mm stack of 12 cylindrical Oxygen-Free High-Conductivity copper electrodes with a diameter of 90 mm is placed in a cylindrical vacuum vessel maintained in UHV conditions, with typical pressures in the 10^{-8}–10^{-9} mbar range. The chamber is in turn surrounded by a coaxial solenoid, which generates a magnetic field B up to 0.2 T providing the radial plasma confinement. Electrodes C1, C2,… to C8 have a length of 90 mm and electrodes S2 and S4 are 150 mm long and are azimuthally sectored in two and four patches, respectively, for excitation and detection purposes. In the typical experimental scheme, the outermost C1 and C8 electrodes are biased to an electrostatic potential V_c between −80 and −100 V and all others are grounded, shaping a potential well where electrons are axially confined. The two grounded outer electrodes GND (90 mm long) and SH (150 mm long) are used to ensure a well-defined potential outside the trapping region. For the low-temperature plasmas here confined, the usual inequality $\omega_c \gg \omega_z \gg \omega_d$ holds, in particular, the cyclotron frequency $\omega_c/2\pi = eB/2\pi m$ (with e and m the electron charge and mass) is in the GHz range, the axial bounce frequency $\omega_z/2\pi$ is in the MHz range, and the diocotron frequency $\omega_d/2\pi = \lambda_p/4\pi^2 B R_W^2 \approx 10 - 100$ kHz, with λ_p the plasma line density and R_W the trap radius. The experimental routine consists in a sequence of production, measurement, and dump (or loss) of plasma, repeated over several cycles, hence the need for stability of plasma generation and experimental conditions in general.

The production of the electron plasma is accomplished by means of a sinusoidal excitation $V_{RF} \sin(\omega_{RF} t)$ applied to one of the inner electrodes, with typical amplitude $V_{RF} \leq 5$ V and frequency $\omega_{RF}/2\pi = 1 - 20$ MHz. When applied in UHV conditions and in the presence of confining potentials, even such a weak drive is able to cause a sufficient heating of free electrons and subsequent ionization of the background gas. An electron plasma column covering the whole transverse section of the trap with an approximately flat profile is reached within a few seconds. More details about the process can be found in Ref. 33.

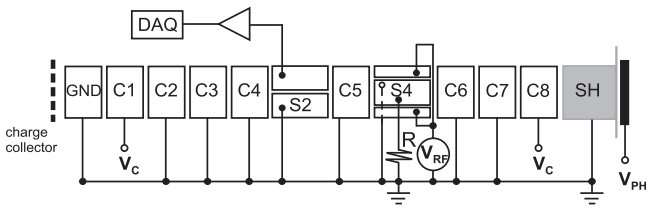

FIG. 1. Experimental set-up. The plasma is confined between the electrodes C1 and C8 biased between –80 and –100 V. A quadrupole radio-frequency excitation of amplitude $V_{RF} = 1 - 5$ V is applied to the opposite sectors S4L, S4R and the diocotron mode is detected on S2T. A planar detector collects the total charge of the electron column.

For this experimental campaign, the drive was applied to two opposite sectors of the S4 electrode (see Fig. 1), thus yielding a RF quadrupolar configuration. In such situation, we have observed the formation of plasma columns with a range of densities and transverse radii. In particular, besides diffuse plasmas occupying the whole trap cross section we could observe the formation of columns with radius $R_p/R_W \simeq 0.1 - 0.2$. Detection of the plasma on a phosphor screen installed at one end of the trap (see Fig. 1) showed that a dynamical equilibrium is reached in a few seconds with the formation of a stable column with typical densities in the 10^6–10^7 cm^{-3} range.[28] We remark that diffuse plasmas have a significantly lower density with respect to the narrow columns created with a quadrupolar drive. The detailed discussion of the formation stage of the plasma column will be the topic of a forthcoming article.

This generation scheme is very sensitive to the experimental conditions, i.e., magnetic field, pressure, and RF drive parameters (frequency, amplitude, and position). This results in experimental difficulties, as these parameters must be adjusted empirically in order to produce a plasma with the desired properties (total charge, mean density, and density profile) and parametric studies (for instance, the dependence of plasma features on the magnetic field strength) may be arduous or impossible, but as the pressure is constant for hours, once the optimal setting is reached the plasma properties are also very stable. The shot-to-shot repeatability was evaluated in previous experiments by means of an optical diagnosis: Dumping the plasma on a phosphor screen set at the end of the electrode stack, we recorded relative variations of the charge distribution below few percents.[28]

The plasma column can be non-destructively monitored by means of electrostatic detection of the transverse (diocotron) modes, which induce a periodic current on sectored electrodes. Specifically, we use here the signal induced on a sector of the S2 electrode (see Fig. 1) to observe the (LF-modulated) plasma rotation around the trap axis, i.e., the $m_\theta = 1$ diocotron mode, whose angular frequency reads

$$\omega_1 = \omega_d/(1 - d^2), \tag{1}$$

if the condition $r_p \doteq R_p/R_W \ll 1$ is satisfied, with $d \doteq D/R_W$ the column radial D displacement normalized to R_W. The total charge of the confined plasma is measured destructively by lowering the confining potential on the C1 electrode so that the plasma is dumped on a 110 mm diameter planar charge collector facing the trap end. The axially integrated electron density profile can also be observed by dumping the plasma on the phosphor screen placed at the other end of the trap and acquiring the phosphor fluorescence with a charge-coupled device (CCD) camera.

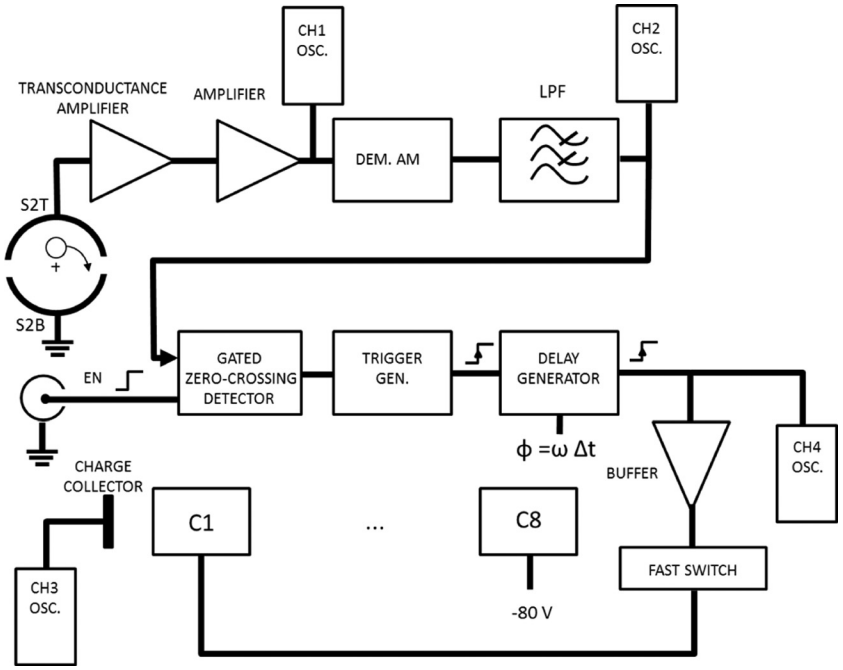

FIG. 2. Phase-charge correlation measurement set-up. The demodulated diocotron signal (detected on the electrode sector S2T) is sent to a gated zero-crossing detector that triggers a delay generator. The output of the delay generator turns on a fast solid-state switch lowering the C1 electrode voltage so that the electron column is dumped onto the charge collector after a time interval $\Delta t = \phi_{LF}/\omega_{LF}$, with ϕ_{LF} and ω_{LF} the phase and frequency of the low-frequency diocotron modulation. The oscilloscope channels CH1, CH2, and CH4 are used to monitor the signals. The total charge is read on channel CH3 as a voltage signal.

While charge and induced-current measurements are independent, a timing and acquisition system was implemented in order to correlate the instantaneous phase of the LF diocotron modulation and the corresponding total charge of the plasma. The measurement scheme is shown in Fig. 2. The amplified electrostatic signal from S2T is demodulated, band-limited at 20 Hz by means of a low-pass filter, and sent to a delay generator in order to synchronize the plasma dump at a set phase. Due to the destructive nature of the total charge measurement, the phase-charge correlation is obtained repeating the production-measurement-dump cycle with different delay times and spanning the phase values ϕ_{LF} in the full range 0–2π, where $\phi_{LF} = 0$ corresponds to the maximum of the electrostatic signal.

III. LOW-FREQUENCY MODULATION

A. Stationary oscillation

In general terms, an amplitude-modulated periodic signal $s(t)$ can be represented by the formula

$$s(t) = [1 + A_{ms} f_{ms}(\omega_{ms} t)] \cdot A_{cs} f_{cs}(\omega_{cs} t), \qquad (2)$$

where the unitary-amplitude periodic functions $f_{cs}(\omega_{cs}t)$ and $f_{ms}(\omega_{ms}t)$ are the carrier and modulating signals, respectively, ω_{cs} and ω_{ms} are their angular frequencies, A_{cs} and A_{ms} are their amplitudes and the modulation index is defined as $h = A_{ms}/A_{cs}$, i.e., the ratio of the modulation amplitude to the pure carrier amplitude. Tuning the RF drive used to generate the plasma column, we have observed the occurrence of a persistent slow modulation of the $m_\theta = 1$ diocotron electrostatic signal (i.e., the carrier signal), with a frequency ω_{LF} typically lying in the Hertz range, i.e., smaller than ω_1 by three orders of magnitude. The envelope of the diocotron signal can have a variety of shapes, which can be roughly divided into quasi-sinusoidal and non-sinusoidal, and with varying degrees of modulation index.

We report here the observations and analysis done on two typical cases, namely, an example of quasi-sinusoidal and of non-sinusoidal modulation. Figure 3 shows a quasi-sinusoidal steady-state LF modulation observed applying a RF drive with $V_{RF} = 2.5$ V and $\omega_{RF}/2\pi = 12$ MHz at a pressure of 5.2×10^{-9} mbar, magnetic field $B = 0.11$ T, and confining potentials $V_c = -80$ V. The signal envelope featuring a modulation index 0.33 and $\omega_{LF}/2\pi = 4.3$ Hz is

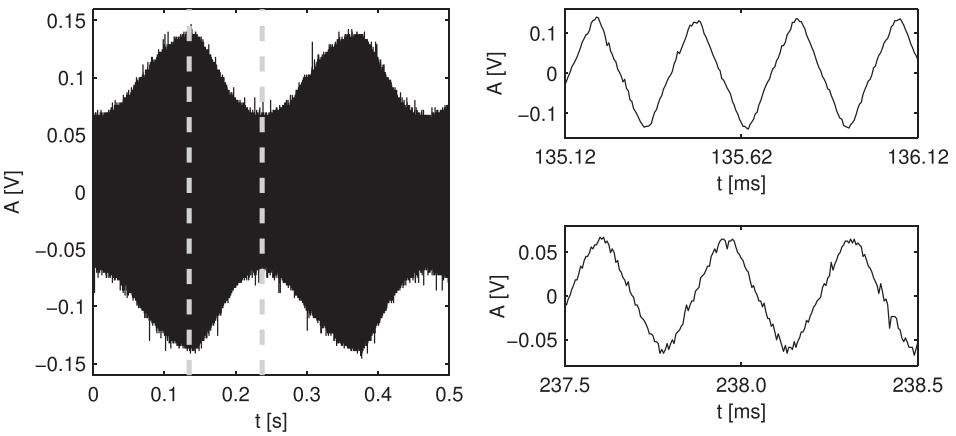

FIG. 3. Induced electrostatic signal of the LF modulated $m_\theta = 1$ diocotron mode. Left panel: The signal envelope over a time span of 0.5 s evidences a LF modulation with period $\tau_{LF} = 0.23$ s and modulation index 0.33. Upper right panel: 1 ms excerpt of the signal at the maximum of the amplitude modulation (first vertical dashed line in the left diagram). The $m_\theta = 1$ mode frequency here is $\omega_1/2\pi = 3.5$ kHz. Lower right panel: 1 ms excerpt at the minimum of the amplitude modulation (second vertical dashed line in the left diagram), with $\omega_1/2\pi = 2.8$ kHz.

visible in the left panel. A 1 ms inset of the signal taken at the maximum and minimum of the amplitude modulation (marked by dashed vertical lines in the diagram) is reported in the upper and lower right panels, respectively. These graphs evidence that the diocotron signal is also frequency-modulated, with $\omega_1/2\pi = 2.8 - 3.5\,\text{kHz}$ and with amplitude peaks (dips) corresponding to frequency peaks (dips). A diocotron signal with $\omega_{LF}/2\pi = 4.4\,\text{Hz}$, amplitude modulation index 0.75, $\omega_1/2\pi = 2.1 - 3.3\,\text{kHz}$, and non-sinusoidal envelope was obtained at $V_{RF} = 2.5\,\text{V}$, $\omega_{RF}/2\pi = 11.8\,\text{MHz}$, $2.8 \times 10^{-9}\,\text{mbar}$, $B = 0.11\,\text{T}$, and confining potentials $V_c = -80\,\text{V}$.

The analysis of the phase-charge correlated measurements is summarized by Fig. 4, where the left and right columns correspond to the quasi-sinusoidal and non-sinusoidal signals, respectively. The LF amplitude modulations are shown in the top row as voltage signal of the electrostatic induced current after demodulation. The second row tracks the trend of the induced diocotron current frequency over a period of the LF oscillation, and the third row shows the correlated variation of the total charge $Q(t)$ of the electron column. One can notice that $\omega_1(t)$ and $Q(t)$ follow similar trends in both cases (with a slight distortion in the frequency trend of the non-sinusoidally modulated signal), which is consistent with the expression of Eq. (1) for ω_1. Nevertheless, the two quantities are not exactly proportional, indicating the presence of other phenomena. This is also confirmed by a strong distortion that is particularly evident in the induced current signal for the non-sinusoidal case, whose trend significantly differs from that of the column charge and first diocotron mode frequency (top-right diagram).

A second series of experiments performed dumping the plasma onto the phosphor screen instead of the charge collector allowed us to obtain information on the plasma offset and its phase correlation with the other quantities of interest. Furthermore, the continuous current of electrons axially escaping the trap and impacting the charge collector was recorded. In this case, a plasma with a diocotron modulation of $\omega_{LF}/2\pi = 6.4\,\text{Hz}$ was generated applying a drive of amplitude $V_{RF} = 3.0\,\text{V}$ and frequency $\omega_{RF}/2\pi = 7\,\text{MHz}$ at a pressure of $2.9 \times 10^{-9}\,\text{mbar}$, magnetic field $B = 0.116\,\text{T}$, and confining potentials $V_c = -90\,\text{V}$. Figure 5 shows the trends of the measured quantities over one modulation period. The top diagram shows the diocotron signal detected from one of the S2 electrode sectors, with a visible amplitude modulation. The second diagram plots the electron current escaping the trap along the longitudinal axis and impacting on the collector. The Fourier analysis of the diocotron signals shows once again the presence of a frequency modulation in the range of 2.9–3.5 kHz, plotted in the third diagram. Repeated experimental cycles with plasma dump on the phosphor screen allowed us to directly measure the offset and the total charge of the dumped plasma, calculated as a sum of the CCD image pixel intensities after subtraction of the background noise. Offset and charge are plotted in the fourth and fifth diagrams, respectively, versus the phase of the LF modulation at the moment of the ejection. One can notice that once again all quantities plotted in this figure are modulated, and in particular, there is an evident phase shift of the offset and escaping current with respect to the amplitude, frequency, and charge modulation. In order to estimate possible radial electron losses, we plot in Fig. 6 the denoised CCD image of the plasma cross section and two typical profiles of electron columns (obtained from a horizontal cut of the images along the plasma center) for plasma columns at maximum and minimum radial displacement. The profile shows a slight increase in mean radius with increasing offset.

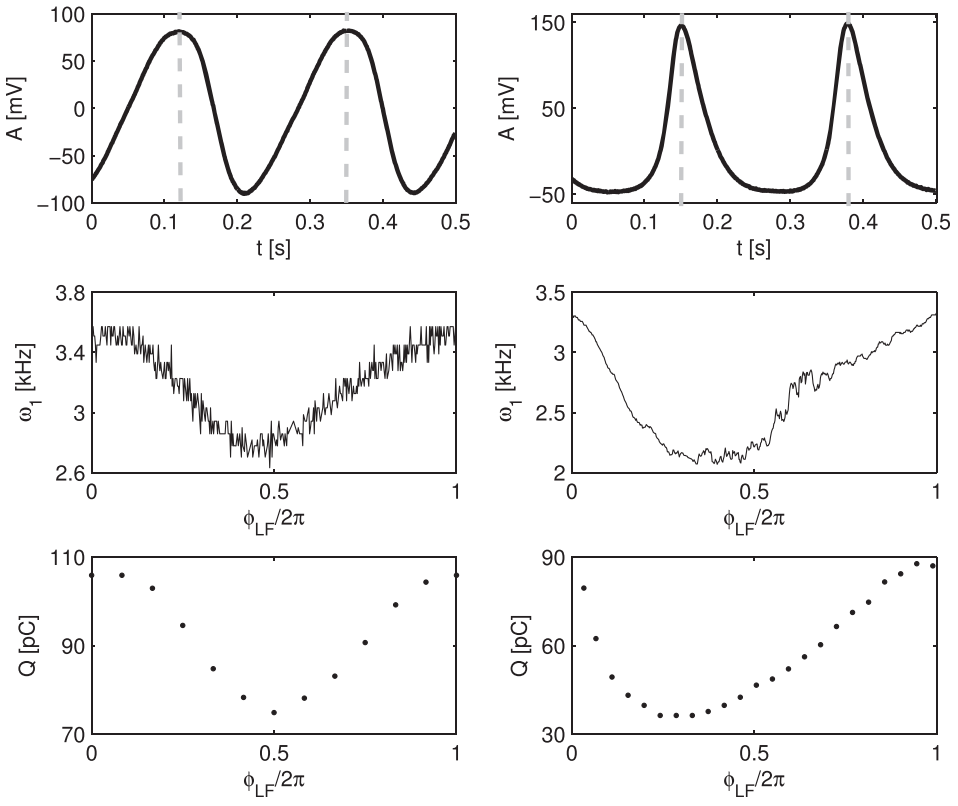

FIG. 4. Analysis of the diocotron signals for two LF modulated electron columns. Left column: Quasi-sinusoidal modulation. Right column: Non-sinusoidal modulation. First row: LF modulation profile, i.e., amplitude modulation of the diocotron signal. Second row: Frequency ω_1 of the diocotron mode, showing the presence of a frequency modulation besides the amplitude oscillation. Third row: Total charge Q of the confined plasma. Charge and diocotron frequency data are obtained by means of the phase-charge correlation technique sketched in Fig. 2. Q and ω_1 are plotted over the phase $\phi_{LF} = \omega_{LF}; \tau_{LF}$ of a complete LF modulation period τ_{LF}, indicated in the top row by the dashed vertical lines.

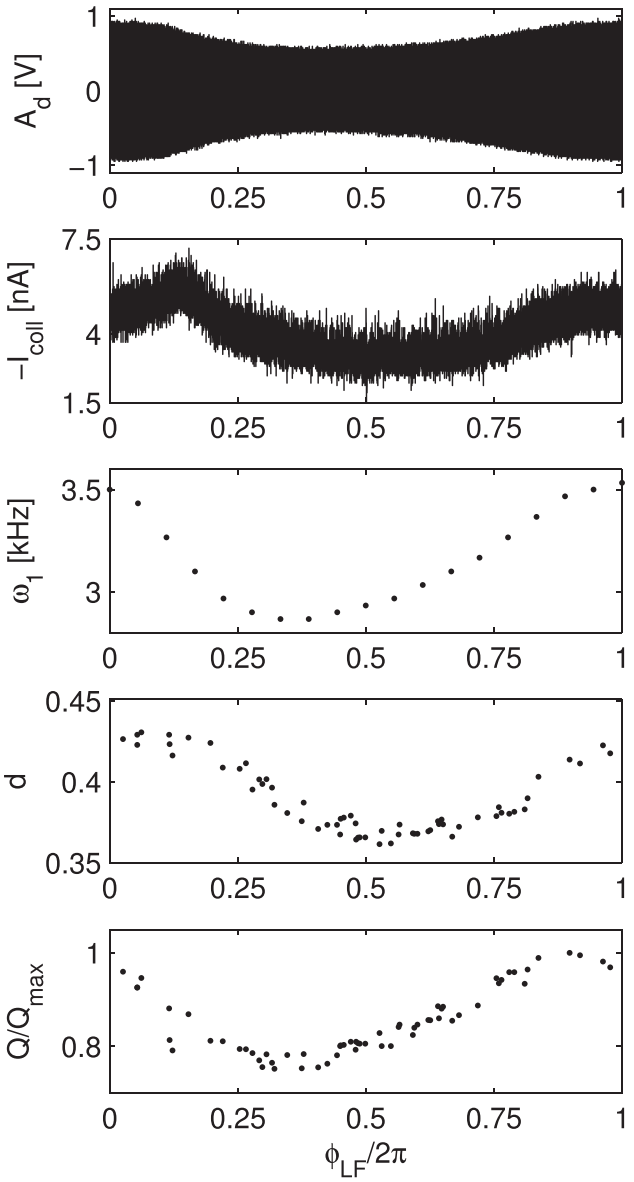

FIG. 5. Modulation of diocotron signal, escaping current, offset, and total confined charge of a LF modulated plasma column. All quantities are plotted over the phase ϕ_{LF} of one LF modulation period. First diagram: $m=1$ diocotron signal measured on a sectored electrode. Second diagram: Electron current I_{coll} escaping axially from the trap to the charge collector. Third diagram: Frequency ω_1 of the diocotron mode. Fourth diagram: Column offset normalized to the trap radius. Fifth diagram: Total charge Q of the confined plasma normalized to the maximum value.

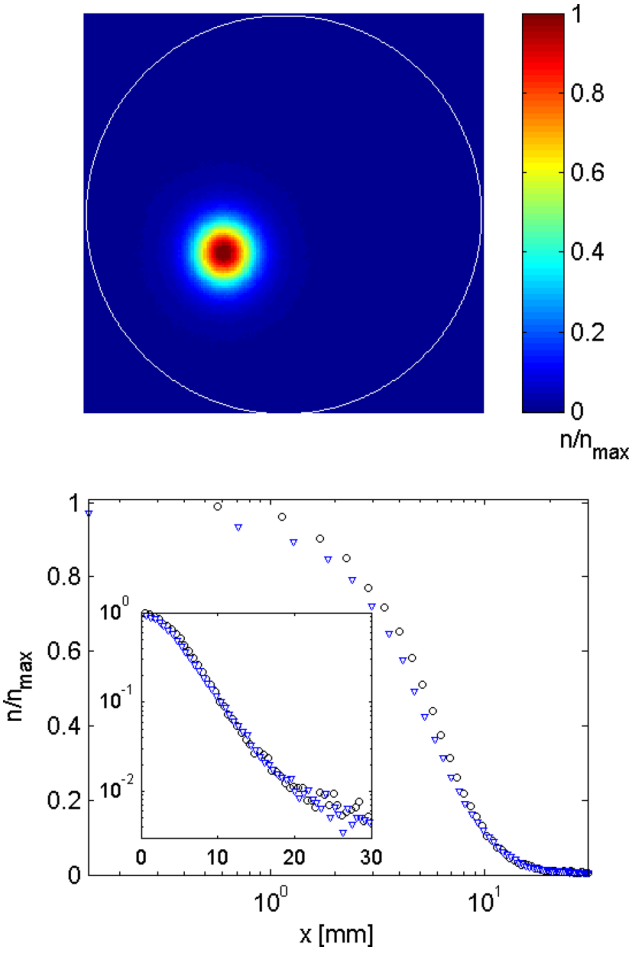

FIG. 6. Visualization of the plasma cross section and profile. Top diagram: denoised CCD image showing the axially integrated electron density n over the trap cross section, normalized to the peak value n_{max}, for a plasma located approximately at the maximum offset. The white circle indicates the trap wall. Bottom diagram: Density profiles of plasmas around the maximum (circles) and minimum offset (triangles), obtained as horizontal cuts along the plasma center. Values are normalized to the peak of the plasma at maximum offset. The logarithmic scale on the vertical axis of the inset evidences a tail smaller by two orders of magnitude than the bulk density.

The typical mean radius of the column is around 5–6 mm. Considering a halo between 20 and 30 mm, its density normalized to the peak value is below 10^{-2} and begins to be comparable with the residual image noise. The total charge in this region is therefore of the order of few percents with respect to the total charge of the column.

The overall interpretation of such observations is not straightforward. A brief discussion is presented in Sec. IV.

B. Damped oscillation

As shown so far, in an experimental configuration where the RF generation drive is continuously applied, an equilibrium is observed where the balance between electron loss and production lasts for hours even in the presence of significant factors known to destabilize the $m_\theta=1$ mode, namely, a resistive wall[19] and positive ions,[21,22] the latter of which are intrinsically present due to the plasma generation mechanism. In order to characterize the features of such configuration, we investigated experimentally the response of the system to external perturbations around an equilibrium condition.

The starting point was an equilibrium where no modulation of the diocotron signal is observed. Like in the cases previously presented, this condition was achieved by empirical adjustment of the experimental parameters (magnetic field, pressure, RF amplitude, and frequency). The system was then perturbed by varying the RF drive amplitude for a finite time interval, and the system's reaction was the insurgence of an underdamped modulation of the diocotron electrostatic signal. An example of such behavior is shown in the left diagram of Fig. 7. Here, the 14 MHz quadrupole RF drive initially set at $V_{RF}=2.5$ V was stepped up to 3.0 V for

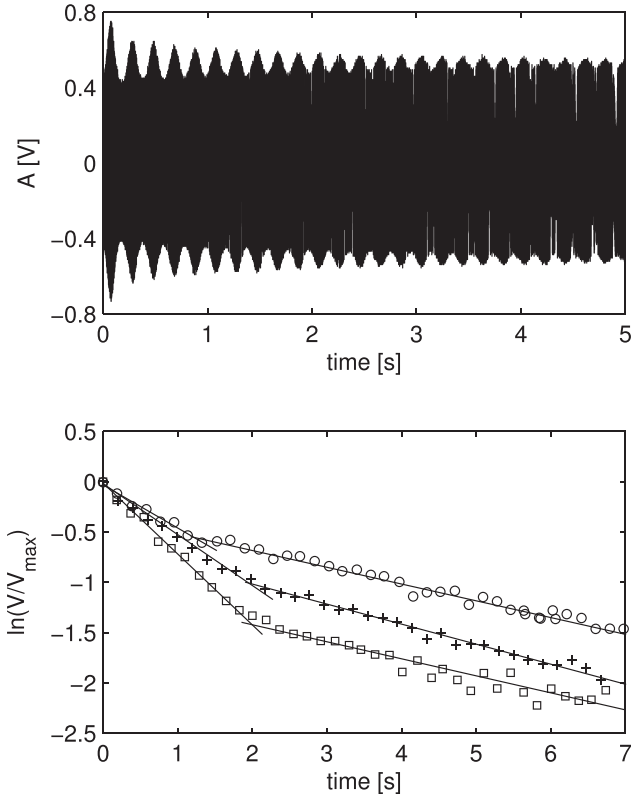

FIG. 7. Top diagram: Electrostatic signal of the $m_\theta = 1$ diocotron mode after a pulsed amplitude perturbation of the RF drive amplitude starting from an initial stable equilibrium in the presence of a resistive load $R_L = 1\,\mathrm{k\Omega}$ applied to an S4 sector. The system response is characterized by an underdamped modulation of the diocotron signal. Bottom diagram: Logarithmic plot of LF modulation amplitude versus time, for $R_L = 1\,\mathrm{k\Omega}$ (crosses), $5\,\mathrm{k\Omega}$ (circles), and $10\,\mathrm{k\Omega}$ (squares). Amplitudes are normalized to the respective maximum values. Each data set is interpolated by two linear (exponential) fitting curves yielding two different decay time constants $\tau_a = 2.0, 2.3, 1.4\,\mathrm{s}$ and $\tau_b = 5.2, 6.1, 5.6\,\mathrm{s}$ for $R_L = 1, 5, 10\,\mathrm{k\Omega}$, respectively.

0.4 s and then brought back to the initial value, maintaining a pressure of 4.2×10^{-9} mbar and a magnetic field of 0.075 T.

We characterized the behavior of the damped LF modulation against the variation of a load resistance R_L connected to the sector S4T of the four-fold split electrode, thus changing the growth rate of the $m_\theta = 1$ diocotron instability. Resistance values spanning the interval from 1 to $10\,\mathrm{k\Omega}$ were used. Within this range, the LF modulation ω_{LF} showed a relative increase of 10% for increasing values of the external load resistor. This trend was fitted by a power law of the type $\omega_{LF} \propto R_L^\gamma + b$ with $\gamma = 0.67$. Notice that the ion instability and the LF modulation are present also for $R_L = 0$ (no resistive instability).

The damping time constants were evaluated by extracting the local maxima of the modulated signals. Figure 7 reports the data versus time on a logarithmic scale for three different resistor values $R_L = 1, 5, 10\,\mathrm{k\Omega}$. A sharp transition between two regimes, both interpolated by a linear (i.e., exponential) fit, is present in all data sets, respectively, at 1.582 s, 1.326 s, and 1.459 s. This may indicate that two different stages, corresponding to different phenomena, take place. The first part shows a faster damping with time constants $\tau_a = 1$–2 s. The second damping regime shows a significantly slower decay and similar time constant values $\tau_b = 5$–6 s, with no apparent trend with respect to R_L. In a quiescent plasma, the growth rate of the $m_\theta = 1$ diocotron mode subject to a resistive load exhibits the well-known resonant peak as a function of the resistor value. Notice that for the typical parameters of these experiments such peak would occur for $R_L \simeq 50 - 200\,\mathrm{k\Omega}$, thus placing the values chosen for R_L in the ascending branch of the instability diagram. Therefore, on the basis of these observations, we find out that such instability growth against R_L is essentially suppressed. This suggests that after the brief initial transient, the system returns to the initial equilibrium state regardless of the specific features and magnitude of the sources of dissipation and instabilities, as they do not significantly affect the damping mechanism while the dominant role is played by the RF excitation and ionization.

IV. DISCUSSION AND CONCLUDING REMARKS

This paper refers to non-neutral plasmas produced by the injection of RF power in Penning-Malmberg traps. It has already been shown that RF-produced electron columns can behave in many respects like the columns produced by thermionic sources and photocathodes: They may exhibit diocotron dynamics, resistive-wall and ion-resonance instabilities, and can be manipulated by applying proper potentials to sectored electrodes (see, e.g., Refs. 28 and 33). In Secs. II and III, we have shown the experimental analysis of a new peculiar behavior of the system, possibly due to the essential role of ionization and RF heating: When the trap is continuously fed by RF power, a periodically oscillating equilibrium is set up, characterized by a smooth periodic variation of the amplitude of the fundamental diocotron mode and a corresponding oscillation of the current flowing out of the trapping region. The relevant periods (30–300 ms) are much longer than those of plasma rotation and collective plasma modes. During the whole evolution, the confined electron column does not crash into the wall as a result of instabilities. The oscillations studied here are quite different from the saw-tooth oscillations of the displacement of an electron column in a cryogenic Penning-Malmberg trap observed by Cluggish and Driscoll[25,34] and interpreted on the basis of a theoretical model (rotational pumping) developed by Crooks and O'Neil.[24] Actually, in our case the effects due to RF power may overcome those due to rotational pumping, and the cooling of the column is mainly due to ionization and energy convection, not to cyclotron emission (our device is at room temperature and the magnetic field is around 0.1 T).

The paper is focused on experimental results. We add here only few remarks that should be taken into account in a theoretical model.

The applied RF power produces the plasma mainly by electron-impact ionization of H_2 molecules. As ions leave the confinement region, a trapped electrons column forms, exhibiting diocotron rotation around the axis of the trap as well as rotation around the center of charge. Note that electrons and ions continuously flow out of the trap, both axially and radially.

In UHV conditions, the energy required to ionize the gas is given to electrons through a stochastic acceleration process, mainly due to the axial component of the RF field.[35] Following this mechanism, the electron distribution function develops a non-Maxwellian tail (on the time scale of the observed slow oscillations) (see, e.g., Ref. 36), and electrons with kinetic energy high enough to overcome the end potential barrier leave the trapping region. In this process, space charge effects and asymmetry of the column ends[21,34] may play an important role. Thus, the energy balance of the electron column is mainly determined by RF heating, cooling via ionizing collisions, and axial energy flux of accelerated electrons leaving the trapping region.

The evolution equation of the angular momentum of the electron plasma that determines the column offset should contain the (stabilizing) effect of the RF field that on the rotation and diocotron time scales (longer than the RF period) acts as a ponderomotive force, the effect of the field of the image charges (destabilizing ion resonance mechanism and stabilizing electron current[37–41]), and the effect of the wall resistance. A stabilizing effect due to the flux-driven damping recently investigated[29] might also be relevant here, since the observed halo (with density somewhat less than 1% of the peak density) can cross the wall during the offset oscillation.

ACKNOWLEDGMENTS

This work was supported by the Italian Ministry for University and Research (MIUR) "PRIN 2009" funds (Grant No. 20092YP7EY) and also received partial support from the INFN, Group V within the "COOLBEAM" project.

[1]J. R. Pierce, *Theory and Design of Electron Beams* (D. Van Nostrand Co., New York, 1949).
[2]J. H. Malmberg and J. S. deGrassie, Phys. Rev. Lett. **35**, 577 (1975).
[3]H. Häffner, T. Beier, S. Djekić, N. Hermanspahn, H.-J. Kluge, W. Quint, S. Stahl, J. Verdú, T. Valenzuela, and G. Werth, Eur. Phys. J. D **22**, 163 (2003).
[4]K. Blaum, Phys. Rep. **425**, 1 (2006).
[5]D. Hanneke, S. Fogwell, and G. Gabrielse, Phys. Rev. Lett. **100**, 120801 (2008).
[6]M. Block, D. Ackermann, K. Blaum, C. Droese, M. Dworschak, S. Eliseev, T. Fleckenstein, E. Haettner, F. Herfurth, F. P. Heßberger, S. Hofmann, J. Ketelaer, J. Ketter, H.-J. Kluge, G. Marx, M. Mazzocco, Yu. N. Novikov, W. R. Plaß, A. Popeko, S. Rahaman, D. Rodríguez, C. Scheidenberger, L. Schweikhard, P. G. Thirolf, G. K. Vorobyev, and C. Weber, Nature **463**, 785 (2010).
[7]M. Amoretti, C. Amsler, G. Bonomi, A. Bouchta, P. Bowe, C. Carraro, C. L. Cesar, M. Charlton, M. J. T. Collier, M. Doser, V. Filippini, K. S. Fine, A. Fontana, M. C. Fujiwara, R. Funakoshi, P. Genova, J. S. Hangst, R. S. Hayano, M. H. Holzscheiter, L. V. Jørgensen, V. Lagomarsino, R. Landua, D. Lindelf, E. Lodi Rizzini, M. Macrì, N. Madsen, G. Manuzio, M. Marchesotti, P. Montagna, H. Pruys, C. Regenfus, P. Riedler, J. Rochet, A. Rotondi, G. Rouleau, G. Testera, A. Variola, T. L. Watson, and D. P. van der Werf, Nature **419**, 456 (2002).
[8]G. Gabrielse, N. S. Bowden, P. Oxley, A. Speck, C. H. Storry, J. N. Tan, M. Wessels, D. Grzonka, W. Oelert, G. Schepers, T. Sefzick, J. Walz, H. Pittner, T. W. Hänsch, and E. A. Hessels, Phys. Rev. Lett. **89**, 213401 (2006).
[9]M. H. Holzscheiter, M. Charlton, and M. M. Nieto, Phys. Rep. **402**, 1 (2004).
[10]R. H. Levy, Phys. Fluids **8**, 1288 (1965).
[11]C. F. Driscoll and K. S. Fine, Phys. Fluids B **2**, 1359 (1990).
[12]K. Fine, A. Cass, W. Flynn, and C. Driscoll, Phys. Rev. Lett. **75**, 3277 (1995).
[13]D. Durkin and J. Fajans, Phys. Fluids **12**, 289 (2000).
[14]Y. Kawai and Y. Kiwamoto, Phys. Rev. E **78**, 036401 (2008).
[15]F. Lepreti, M. Romé, G. Maero, B. Paroli, R. Pozzoli, and V. Carbone, Phys. Rev. E **87**, 063110 (2013).
[16]A. G. Marshall, C. L. Hendrickson, and G. S. Jackson, Mass Spectrom. Rev. **17**, 1 (1998).
[17]M. Audi and M. de Simon, Vacuum **37**, 629 (1987).
[18]C. F. Driscoll and J. H. Malmberg, Phys. Rev. Lett. **50**, 167 (1983).
[19]W. D. White, J. H. Malmberg, and C. F. Driscoll, Phys. Rev. Lett. **49**, 1822 (1982).
[20]G. Bettega, F. Cavaliere, B. Paroli, R. Pozzoli, M. Romé, and M. Cavenago, Phys. Plasmas **15**, 032102 (2008).
[21]A. J. Peurrung, J. Notte, and J. Fajans, Phys. Rev. Lett. **70**, 295 (1993).
[22]G. Bettega, F. Cavaliere, M. Cavenago, A. Illiberi, R. Pozzoli, and M. Romé, Plasma Phys. Controlled Fusion **47**, 1697 (2005).
[23]X.-P. Huang, F. Anderegg, E. M. Hollmann, C. F. Driscoll, and T. M. O'Neil, Phys. Rev. Lett. **78**, 875 (1997).
[24]S. M. Crooks and T. M. O'Neil, Phys. Plasmas **2**, 355 (1995).
[25]B. P. Cluggish, C. F. Driscoll, K. Avinash, and J. A. Helffrich, Phys. Plasmas **4**, 2062 (1997).
[26]A. A. Kabantsev and C. F. Driscoll, Phys. Rev. Lett. **97**, 095001 (2006).
[27]A. A. Kabantsev, D. H. E. Dubin, C. F. Driscoll, and Yu. A. Tsidulko, Phys. Rev. Lett. **105**, 205001 (2010).
[28]G. Maero, B. Paroli, R. Pozzoli, and M. Romé, Phys. Plasmas **18**, 032101 (2011).
[29]A. A. Kabantsev, C. Y. Chim, T. M. O'Neil, and C. F. Driscoll, Phys. Rev. Lett. **112**, 115003 (2014).
[30]M. Maggiore, M. Cavenago, M. Comunian, F. Chirulotto, A. Galatà, M. De Lazzari, A. M. Porcellato, C. Roncolato, S. Stark, A. Caruso, A. Longhitano, F. Cavaliere, G. Maero, B. Paroli, R. Pozzoli, and M. Romé, Rev. Sci. Instrum. **85**, 02B909 (2014).
[31]G. Maero, M. Romé, F. Lepreti, and M. Cavenago, Eur. Phys. J. D **68**, 277 (2014).
[32]G. G. M. Coppa, A. D'Angola, and R. Mulas, Phys. Plasmas **19**, 062507 (2012).
[33]B. Paroli, F. De Luca, G. Maero, R. Pozzoli, and M. Romé, Plasma Sources Sci. Technol. **19**, 045013 (2010).
[34]B. P. Cluggish and C. F. Driscoll, Phys. Plasmas **3**, 1813 (1996).
[35]G. Maero, B. Paroli, R. Pozzoli, and M. Romé, "Modelling of electron heating in a Penning-Malmberg trap by means of a chaotic map," in *Proceedings of the 41st EPS Conference on Plasma Physics, Europhysics Conference Abstracts* (2014), Vol. 38F, P4.127.
[36]M. A. Lieberman and V. A. Godyak, IEEE Trans. Plasma Sci. **26**, 955 (1998).
[37]A. J. Peurrung and J. Fajans, Phys. Fluids B **5**, 4520 (1993).
[38]J. Fajans, Phys. Fluids B **5**, 3127 (1993).
[39]A. A. Kabantsev and C. F. Driscoll, AIP Conf. Proc. **692**, 61 (2003).
[40]A. A. Kabantsev and C. F. Driscoll, Rev. Sci. Instrum. **75**, 3628 (2004).
[41]A. A. Kabantsev and C. F. Driscoll, Trans. Fus. Sci. and Tech. **51**, 96 (2007).